JCTC Journal of Chemical Theory and Computation
Article
pubs.acs.org/JCTC

An On-the-Fly Surface-Hopping Program JADE for Nonadiabatic Molecular Dynamics of Polyatomic Systems: Implementation and Applications

Likai Du[†,‡,§] and Zhenggang Lan*[,†,‡,§]

[†]Key Laboratory of Biobased Materials, Qingdao Institute of Bioenergy and Bioprocess Technology, Chinese Academy of Sciences, Qingdao, 266101 Shandong, People's Republic of China

[‡]University of Chinese Academy of Sciences, Beijing 100049, People's Republic of China

[§]The Qingdao Key Lab of Solar Energy Utilization and Energy Storage Technology, Qingdao Institute of Bioenergy and Bioprocess Technology, Chinese Academy of Sciences, Qingdao, 266101 Shandong, People's Republic of China

S Supporting Information

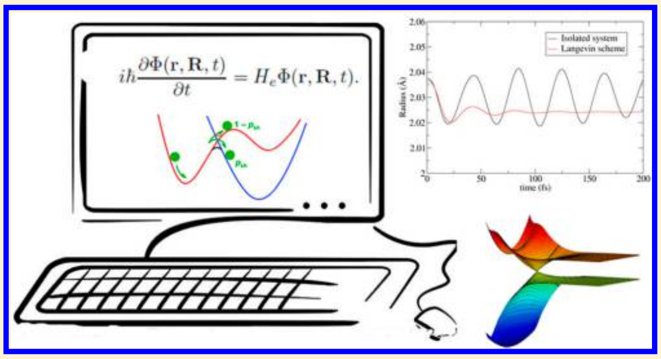

ABSTRACT: Nonadiabatic dynamics simulations have rapidly become an indispensable tool for understanding ultrafast photochemical processes in complex systems. Here, we present our recently developed on-the-fly nonadiabatic dynamics package, JADE, which allows researchers to perform nonadiabatic excited-state dynamics simulations of polyatomic systems at an all-atomic level. The nonadiabatic dynamics is based on Tully's surface-hopping approach. Currently, several electronic structure methods (CIS, TDHF, TDDFT(RPA/TDA), and ADC(2)) are supported, especially TDDFT, aiming at performing nonadiabatic dynamics on medium- to large-sized molecules. The JADE package has been interfaced with several quantum chemistry codes, including Turbomole, Gaussian, and Gamess (US). To consider environmental effects, the Langevin dynamics was introduced as an easy-to-use scheme into the standard surface-hopping dynamics. The JADE package is mainly written in Fortran for greater numerical performance and Python for flexible interface construction, with the intent of providing open-source, easy-to-use, well-modularized, and intuitive software in the field of simulations of photochemical and photophysical processes. To illustrate the possible applications of the JADE package, we present a few applications of excited-state dynamics for various polyatomic systems, such as the methaniminium cation, fullerene (C_{20}), p-dimethylaminobenzonitrile (DMABN) and its primary amino derivative aminobenzonitrile (ABN), and 10-hydroxybenzo[h]quinoline (10-HBQ).

1. INTRODUCTION

The photoinduced electronic excitation of molecular systems leads to a complex sequence of dynamics,[1−4] such as radiative electronic transitions (fluorescence, phosphorescence), nonradiative electronic transitions (internal conversions, intersystem crossings), electron and energy transfers, chemical reactions, etc. These photophysical and photochemical processes are extremely important for the evolution of life and living environments. Thus, great efforts have been made in recent decades to investigate various important photoinduced processes.[3−5] One of the most fundamental phenomena in photophysics and photochemistry is the so-called "nonadiabatic process,"[4−6] which refers to the electronic transition between different Born−Oppenheimer (BO) potential energy surfaces (PES). Such nonadiabatic transitions become ultrafast when two electronic states approach or cross each other along the nuclear coordinates. When two electronic states of the same multiplicity become degenerate, the so-called "conical intersection" is formed. The nonadiabatic transitions in the vicinity of the conical intersections between different electronic states are at the heart of photochemistry, internal conversion, fluorescence quenching, and nonradiative energy dissipation processes.[5,7−15]

In principle, the theoretical description of nonadiabatic processes between different electronic states with the same multiplicity represents a great challenge because the presence of strong coupling between the nuclear and electronic motions leads to the breakdown of the BO approximation.[3] An exact description of the non-BO dynamics is offered by the full solution of the time-dependent Schrödinger equation for strongly coupled electron−nucleus systems. However, the high computational costs of the complete quantum-mechanical solution and the need for the construction of the relevant PES prior to propagation limit its applications to small systems with only a few nuclear degrees of freedom. Many other alternative

Received: December 7, 2014
Published: February 24, 2015

ACS Publications © 2015 American Chemical Society

DOI: 10.1021/ct501106d

schemes have also been proposed to describe the nonadiabatic dynamics within the framework of quantum evolution, such as the multiconfiguration time-dependent Hartree (MCTDH) approach,[16] the multilayer MCTDH treatment,[17,18] and the full multiple spawning (FMS) and related methods.[19−21] In practice, some semiclassical nonadiabatic approaches have been developed due to their potential application to larger molecules.[5] More accurate semiclassical approaches have been proposed, such as the quantum-classical Liouville descriptions[22,23] and the hydrodynamic nonadiabatic dynamics;[24,25] however, numerical instability limits their widespread applications. The semiclassical initial value representation (SC-IVR) and its extensions, developed by Miller and co-workers, are also practical approaches that can successfully incorporate quantum effects into molecular dynamics simulations.[26−28] However, a large number of trajectories must be computed, which requires huge computational costs for complex systems. In semiclassical dynamics, there are two widely applied methods, i.e., the so-called "Ehrenfest" or "mean-field" method[29−31] and the trajectory surface-hopping method,[13,32−34] and their mixed/extension schemes.[35−38] The standard mean-field method leads to the evolution of the system on the averaged PES in regions of weak coupling, which is undesirable for simulating photochemistry. The surface-hopping method, due to its conceptual simplicity, computational efficiency, as well as easy implementation, is one of the most successful semiclassical approaches.

The choice of quantum chemistry methods for solving the electronic structure problem is a crucial issue in the application of nonadiabatic dynamics methods. The balance between computational accuracy and cost should be largely considered. To study medium- to large-sized molecular systems, the excited-state electronic structure calculations should be fast enough to allow the efficient computation of the large number of geometries while adequate accuracy should also be achieved, even at strongly distorted nuclear geometries. Unfortunately, it is not straightforward to find a suitable excited-state method that can satisfy all these requirements at once. The more reliable high-level *ab initio* methods with high accuracy[39−41] (such as CASSCF,[42] CASPT2,[43−45] MR-CISD[46]) are restricted to small systems due to their high computational cost and high scaling. The cheaper semiempirical methods[47,48] (such as OM2/MRCI,[49,50] AM1/CIS[51,52]) are limited by their parameter-dependent performance. Up to medium-sized molecular systems, the single-reference methods,[41,53−60] such as EOM-CC, CC2, ADC(3), ADC(2), and TDDFT, are possible candidates for excited-state calculations. In the past years, the TDDFT method has become the most widely used approach in the calculation of the excited states of medium to large molecular systems due to its good trade-off between computational cost and accuracy. The accuracy of TDDFT is debated in terms of issues such as long-range charge-transfer (CT) excited states[58,61−63]and excited states dominated by double excitations.[64] Moreover, the limitations of linear-response TDDFT to describe conical intersections between the first excited state and the ground state (S_0/S_1) have been critically examined in the literature.[58,63−66] However, TDDFT is still the most applicable method (scaling as N^4, N is the total basis size) for systems as large as organic oligomers or the transition metal centers in enzymes. Thus, great efforts have been made to improve the performance of TDDFT. For instance, the performance and accuracy have been steadily improved by many novel exchange-correlation functionals, especially to treat the CT excitation problems with range-separated functionals.[67,68] The Tamm−Dancoff approximation (TDA) was reported to improve the description of S_0/S_1 conical intersections.[64] Certainly, TDDFT may be more reliable to treat the conical intersections between different excited states. Currently, the TDDFT method is available in many quantum chemistry (QC) packages. Thus, it should be highly interesting to connect nonadiabatic dynamics with TDDFT, even though up to now only a few groups reported the successful case studies of nonadiabatic dynamics at the TDDFT level.[66,69−74]

The inclusion of environmental effects, such as solvents, may have a significant influence on photochemical processes.[75,76] One possible solution to treat the environment is the hybrid QM/MM scheme.[77−85] However, the setup of the QM/MM model is often cumbersome because of the explicit description of the entire environment at the atomic/molecular level. Alternatively, the Langevin dynamics (LD) scheme is an important extension of Newton's equation, which can be applied to treat environment effects in a simple and implicit manner.[86,87] Thus, the introduction of LD into nonadiabatic dynamics should in principle be an efficient way to account for the influence of environmental degrees of freedom if all the parameters are properly chosen. In general, the LD scheme is a very easy-to-use option to semiquantitatively predict many condensed-phase photodynamics processes, for instance, the energy transfer from excited chromophores to the medium.[88−91]

The calculation of the PES is another important technical issue in nonadiabatic dynamics simulations, and two general strategies are often employed, namely the "PES-fitting" strategy or the "direct" strategy.[92] In the "PES-fitting" strategy, the PES of electronic states and the interstate couplings are represented as functions of nuclear coordinates based on prior electronic structure calculations. This approach may be extremely expensive for polyatomic molecular systems with many nuclear degrees of freedom. In the direct strategy, also known as "on-the-fly," the PES and interstate couplings are computed at every step of the molecular dynamics, which is especially suitable for trajectory-based methods[92] and is also applicable to quantum dynamics with traveling localized basis functions.[19−21] The use of well-defined classical trajectories in the surface-hopping method makes it possible to employ direct dynamics,[13] in which the energies, gradients, and nonadiabatic couplings are calculated at each point along the trajectory. Such direct dynamics approaches are extremely suitable for understanding complex ultrafast photochemistry processes in realistic polyatomic systems,[92] for which the PES is generally very complicated.

The direct dynamics method can be implemented in different manners. One approach is to add the dynamics module directly into an electronic structure program, such as the implementation of the trajectory surface-hopping (TSH) method in CPMD,[93] Turbomole,[94] and MNDO,[95] and the FMS approach in Molpro.[21,96] Although this implementation provides maximum computational efficiency, it would be strongly dependent on the specificities of a QC package. For example, the TSH method in CPMD can only use the TDDFT method based on plane-wave basis sets,[93] which is more suitable for extended periodic systems. Furthermore, the choice of the exchange-correlation functional is also very limited, and specifically, range-separated functionals (important for the CT excitations[67,68]) are not yet included in the public version of the CPMD code. The limited choice in functionals is also true for the TSH dynamics in Turbomole. In addition, the currently implemented TSH algorithm in Turbomole can only handle switches between the first excited singlet state and the ground state.[70] The TSH dynamics in the MNDO code only works with semiempirical electronic structure methods (i.e., OM2/MRCI);[95] thus, the results are highly dependent on the applicability and accuracy of the parameters.

Another direct dynamics implementation is to combine the evolution of the dynamics and the QC calculations in a modular fashion. This modular approach appears to be more appealing in facilitating the incorporation of new features in various QC packages, although the communication between the evolution of the dynamics and the QC calculations requires a relatively small amount of extra computational cost. A few programs (such as PYXAID,[97] SHARC,[98] and Newton-X[99,100]) for nonadiabatic dynamics simulations are organized in a modular fashion with their own features. For example, the PYXAID program, based on the classical path approximation (CPA) and the electronic transitions between different Kohn–Sham orbitals, is suggested to be suitable for condensed matter systems and requires that the electronic excitation does not result in significant structural changes.[97] Although the SHARC program is proposed to be able to treat arbitrary couplings in molecular systems, it interfaces to only a few high-level *ab initio* methods (i.e., CASSCF and MRCI) in MOLPRO, MOLCAS, and COLUMBUS. Currently, the TSH method at the TDDFT level is not supported in the SHARC program. Because only high-level correlated methods are allowed, most of the recent studies focus on relatively small systems.[98,101]The Newton-X code is proposed to be a package for Newtonian dynamics close to the crossing seam[98,99] and originally supports the TSH dynamics with a few multireference methods. Recently, dynamics studies with single-reference methods (TDDFT and ADC(2)) were also reported.[73]Generally speaking, there is still much room for the improvement of the algorithms, for the development of elaborate program packages to achieve more efficient applications, for the possible extension of novel trajectory-based dynamics methods and state-of-art electronic structure methods, and for better performance with large molecular systems.

In this paper, we report a new package "JADE" for this purpose, which is also designed to work in the modular manner and to loosely link to available electronic structure packages. Currently, the rich interfaces allow us to use the TDDFT (both TDA and RPA), TDHF, CIS, and ADC(2) methods in several packages (Turbomole, Gaussian, and GAMESS (US)). Importantly, some additional features are provided. For instance, compared with Newton-X, the Langevin dynamics (LD) is implemented in the JADE package as an alternative to Newtonian dynamics and is an easy-to-use tool to account for the environmental effects. More sampling methods of the initial conditions are also provided, which includes Wigner sampling, transition state sampling, and so on (see discussions below). In this work, the developed nonadiabatic dynamics codes, within Tully's trajectory surface-hopping (TSH) method,[13] are implemented on the basis of the "on-the-fly" calculation of electronic quantities. The propagation of electronic motion in the JADE package is implemented in terms of the evolution of the density matrix. The program is written in the Fortran and Python programming languages in the concept of modularity. The code has been interfaced with Turbomole,[102] Gaussian,[103] and Gamess (US).[104] Because the JADE code aims to perform nonadiabatic dynamics simulations of complex polyatomic systems at the all-atom level, several single-reference methods, such as CIS, TDHF, TDDFT (RPA and TDA), and ADC(2), were implemented. It is also very feasible to develop new interfaces for other excited-state methods or QC packages in a consistent fashion. Meanwhile, other trajectory methods, such as the Ehrenfest method, can be easily incorporated. The Langevin dynamics (LD) is implemented as an easy-to-use tool for an approximated incorporation of environmental effects. Additionally, various initial sampling methods are implemented, and a few statistical analysis tools are supported. The performance of the surface-hopping dynamics and the LD scheme are examined for the excited-state dynamics of various molecular systems.

2. THEORY AND METHODS

2.1. Surface-hopping Dynamics. In the TSH method, the nuclear and electronic degrees of freedom are treated by classical and quantum dynamics, respectively. The nuclear degrees of freedom are propagated by independent classical trajectories $\mathbf{R}(t)$ on the currently occupied electronic state, which is computed by the numerical integration of Newton's equations. The velocity-Verlet algorithm[105,106] is used for nuclear propagation.

The electronic wave function $\Phi(\mathbf{r},\mathbf{R},t)$ obeys the time-dependent Schrödinger equation

$$i\hbar\frac{\partial\Phi(\mathbf{r},\,\mathbf{R},\,t)}{\partial t} = \mathbf{H_e}\Phi(\mathbf{r},\,\mathbf{R},\,t) \tag{1}$$

where $\mathbf{r}$ and $\mathbf{R}$ are the coordinates of the n electrons and N nuclei system, respectively. $\mathbf{H_e}$ is the electronic Hamiltonian, which is time-dependent through $\mathbf{R}(t)$. The electronic wave function can be expanded in a set of known electronic basis sets (φ_i).

$$\Phi(\mathbf{r},\,\mathbf{R},\,t) = \sum_i c_i(t)\varphi_i(\mathbf{r},\,\mathbf{R}) \tag{2}$$

And $c_i(t)$ represents the expansion coefficients of the electronic wave function. Then, the propagation of the quantum amplitudes along the nuclear trajectory $\mathbf{R}(t)$ can be given.

$$i\hbar\frac{dc_j(t)}{dt} = \sum_i c_i(t)[H_{ji} - i\hbar\mathbf{v}\cdot\mathbf{F}_{ji}] \tag{3}$$

$$H_{ji} \equiv \langle\varphi_j|H_e|\varphi_i\rangle \tag{4}$$

$$\mathbf{F}_{ji} \equiv \langle\varphi_j|\nabla_{\mathbf{R}}|\varphi_i\rangle \tag{5}$$

In eq 3, $\mathbf{v}$ is the vector of nuclear velocities, and H_{ij} and $\mathbf{F}_{ji}$ are the electronic Hamiltonian and nonadiabatic coupling matrix elements between states j and i, respectively. The integration of eq 3 is carried out numerically in the JADE program by performing a unitary propagation of the quantum amplitudes.[5]

The nonadiabatic coupling terms can be reformulated as the scalar product of the velocity vector $\mathbf{v}$ and the nonadiabatic coupling vector $\mathbf{F}_{ji}$.[107]

$$\sigma_{ji}(t) \equiv \mathbf{v}\cdot\mathbf{F}_{ji} = \langle\varphi_j|\frac{\partial}{\partial t}|\varphi_i\rangle \tag{6}$$

The transition probability of jumping from one potential energy surface to another is evaluated on the basis of Tully's fewest switches algorithm. Therefore, the probability for a transition from i to j is

$$P_{ij} = \frac{2\int_t^{t+\Delta t} \mathrm{d}t[\hbar^{-1}Im(c_i^* c_j H_{ij}) - Re(c_i^* c_j \mathbf{v}\cdot\mathbf{F}_{ji})]}{|c_i(t)|^2} \tag{7}$$

To avoid a negative (unphysical) value of P_{ij}, the hopping probability can be defined as

$$g_{ij} = \max(P_{ij}, 0) \tag{8}$$

Then, a uniform random number $0 < \xi < 1$ is generated at each time step, and the hopping from state i to state k is performed if

$$\sum_{j=1}^{k} g_{ij} < \xi < \sum_{j=1}^{k+1} g_{ij} \tag{9}$$

The density matrix representation was adopted in our implemented code, so that eq 3 can be rewritten in terms of the density matrix elements $\rho_{kj} \equiv c_k c_j^*$

$$\begin{aligned} i\hbar\frac{d\rho_{kj}}{dt} &= \sum_l [\rho_{lj}(H_{kl} - i\hbar\mathbf{v}\cdot\mathbf{F}_{kl}) - \rho_{kl}(H_{lj} - i\hbar\mathbf{v}\cdot\mathbf{F}_{lj})] \\ &= [\mathbf{H} - i\hbar\mathbf{v}\cdot\mathbf{F}, \boldsymbol{\rho}]_{kj} \end{aligned} \tag{10}$$

In the adiabatic representation, the electronic wave functions are eigenfunctions of the electronic Hamiltonian, and the Hamiltonian matrix (H_{ji}) is diagonal with nonzero elements equal to the eigenenergies ε_i.

$$H_{ji} = \varepsilon_i \delta_{ji} \tag{11}$$

Then, the hopping probability in the adiabatic representation becomes

$$P_{ij} = \frac{2\Delta t Re(\rho_{ij})\mathbf{v}\cdot\mathbf{F}_{ji}}{\rho_{ii}} \tag{12}$$

In the TSH method, the quantum amplitudes propagated along a single trajectory $\mathbf{R}(t)$ and the amplitudes $c_i(t)$ of all the other states are also artificially restricted to be propagated along $\mathbf{R}(t)$. This causes the so-called "over-coherence problems" that refer to the nondecaying feature of ρ_{ij} during the TSH propagation.[38,108−111] A few corrections have been proposed[112−117] to account for the decoherence effects. Currently, we employ a practical way proposed by Granucci and Perciso to add "decoherence effects."[115] The instantaneous hops from one PES to another are controlled by a stochastic switching algorithm.

In the JADE package, the velocity adjustment is performed after a successful hop to conserve the total energy. If the analytic nonadiabatic coupling vector is available, the velocities can be rescaled in the direction of the nonadiabatic coupling vector, and this choice is suggested by semiclassical analogies.[34,118] When the numerical nonadiabatic coupling vector with respect to time is available, the conservation of energy is imposed by uniformly rescaling the nuclear velocities.[119]

2.2. Numerical Computations of Nonadiabatic Coupling Terms.

The nonadiabatic TSH dynamics in the adiabatic representation requires the explicit calculation of nonadiabatic couplings (NAC). Two approaches are possible, namely the analytic and numerical calculations of the NAC terms. Here, we provide a brief introduction of the NAC calculations at the TDDFT level. Several theoretical efforts have been made to formulate the analytical NAC within the framework of frequency domain TDDFT.[120−132] However, the analytic NAC between two arbitrary electronic states within the TDDFT are not commonly available in most of the standard QC packages. An alternative choice is to evaluate the numerical nonadiabatic couplings and calculate the derivative of the electronic wave function with respect to time.[107,125] In practice, the finite difference scheme was used to evaluate the NAC matrix elements at the TDDFT level with the following relationship, which is particularly suitable if the NAC matrix elements cannot be directly calculated using electronic structure methods.[99,119,133−136]

$$\sigma_{ji}\left(t + \frac{\Delta t}{2}\right) = \frac{\langle\varphi_i^*(t)|\varphi_j(t + \Delta t)\rangle - \langle\varphi_i^*(t + \Delta t)|\varphi_j(t)\rangle}{2\Delta t} \tag{13}$$

where Δt is the time step used for the integration of Newton's classical equations of motion. In this approach, the true change in the electronic wave functions over the entire time step is resolved by computing the overlap integrals between the adiabatic wave functions of different electronic states at times t and $t + \Delta t$.[136] The electronic ground state can be represented by a single Slater determinant built from the occupied Kohn−Sham orbitals, while the wave functions of the excited electronic states can be approximated by the expansion of singly excited configurations. It is worth noting that the expansion coefficients for the excited state K can be obtained according to Casida's assignment ansatz.[137] The wave function Ψ_K is written as a formal configuration interaction with single excitations, namely the CIS form[73,119,125,138]

$$|\Psi_K(\mathbf{r}; \mathbf{R}(t))\rangle = \sum_{i,a} c_{i,a}{}^K |\Phi_{ia}{}^{\mathrm{CSF}}(\mathbf{r}; \mathbf{R}(t))\rangle \tag{14}$$

$$c_{i,a}{}^K = \sqrt{\frac{\varepsilon_a - \varepsilon_i}{\omega_K}}(\mathbf{X} + \mathbf{Y})_{i,a}{}^K \tag{15}$$

In eq 15, ε_a and ε_i are the energies of the virtual and occupied molecular orbitals, respectively, and ω_K is the corresponding excitation energy. **X** and **Y** represent the solutions of the TDDFT/RPA or TDHF eigenvalue problem.[58,137] In the case of TDDFT/TDA and CIS, only **X** vectors are available. Our implementation of nonadiabatic dynamics in the JADE package is based on localized atomic basis sets. Technical details for computing the NAC in the JADE package are summarized in the Supporting Information. Furthermore, different means of obtaining the expansion coefficients ($c_{i,a}{}^K$) have been reported.[119,125,135,138,139] In this work, several options are examined and summarized in the Supporting Information.

In the ADC(2) method, the approximated excited-state wave functions are constructed. For simplicity, the single-excitation response coefficients are used to construct a formal CIS wave function. The interface to the ADC(2) method is currently available for the Turbomole package. Such an approach has also been reported in a recent study.[73]

2.3. Langevin Dynamics.

The energy relaxation effect, which plays an important role in photochemical processes, can be approximately accounted for in the simulation using the Langevin equation. In principle, Langevin dynamics (LD) mimics the viscous aspect of a solvent by including two additional force terms in the standard equation of Newton's second law, namely,

$$M\frac{d^2\mathbf{R}(t)}{dt^2} = -\nabla V(\mathbf{R}(t)) - \gamma M\frac{d\mathbf{R}(t)}{dt} + \sqrt{2\gamma k_B TM}\mathbf{X}(t) \tag{16}$$

In the above equation, $\nabla\mathbf{V}$ is the gradient of the system and γ represents the frictional drag on the system. T is the temperature and k_B is Boltzmann's constant. Thus, the LD scheme is characterized by the use of stochastic terms to describe the environment effects. If all the parameters are properly chosen, the influence of the solvent's degrees of freedom on the system under investigation should be reasonably described. For example, the value of $\gamma = 50$ ps^{-1} is close to the viscosity of water molecules (approximately 1 mPa·s).[87,140] Moreover, the random forces $\mathbf{X}(t)$ are represented as a white-noise field, which has an expected value of zero and displays no correlation between two successive time steps.

$$\langle X(t)\rangle = 0 \tag{17}$$

$$\langle X(t)\, X(t')\rangle = \delta(t - t') \tag{18}$$

where δ is the Dirac delta function.

In general, the dynamical and structural properties obtained from the LD simulation should agree quite well with similar properties obtained from explicit solvent simulations if a suitable collision frequency is adopted.[86,141] Additionally, the LD approach allows for temperature control, for example via a thermostat, thus approximating the thermodynamics limit of the canonical ensemble. Currently, we have implemented the LD method in the JADE code and applied it to the study of several model systems.

2.4. Initial Conditions.

In TSH methods, different internal conditions are required to mimic the distribution in the phase space. Usually, an ensemble of initial conditions (i.e., coordinates and momenta and starting electronic state) can be prepared, using the classical distribution function in the phase space to mimic the initial nuclear quantum wave packet on the chosen electronic state. The JADE program offers various procedures to perform the initial sampling for TSH dynamics.

For the vibrational ground state, the initial conditions can be sampled by the Wigner function. In the 1930s, Wigner[142] proposed that one can obtain the quantum mechanical averages of $\mathbf{Q}$ and $\mathbf{P}$ dependent quantities in a classical framework by using a suitably defined pseudodistribution $\rho_W(\mathbf{Q},\mathbf{P})$. If we assume a quadratic approximation for the PES around the minimum, the all internal coordinates can be described by the normal modes $3N - 6$ (or $3N - 5$)$\mathbf{Q}$ (N is the number of atoms), and the quasi-classical phase-space distribution can be approximated by a Wigner distribution

$$\rho_w(\mathbf{Q}_i, \mathbf{P}_i) = (\pi\hbar)^{-1}\int d\eta\chi_0^*(\mathbf{Q}_i + \eta)\,\chi_0(\mathbf{Q}_i - \eta)e^{2i\eta\mathbf{P}_i/\hbar} \tag{19}$$

where χ_0 is the quantum harmonic oscillator wave function for the vibrational ground state and $\mathbf{P}_i$ is the momentum associated with the normal coordinate $\mathbf{Q}_i$. The evaluation of this integral gives

$$\rho_W(\mathbf{Q}_i, \mathbf{P}_i) = (\pi\hbar)^{-1}\exp(-\mu_i\omega_i\mathbf{Q}_i^{\,2}/\hbar)\,\exp(-\mathbf{P}_i^2/(\mu_i\omega_i\hbar)) \tag{20}$$

in which μ_i is the reduced mass and ω_i is the harmonic frequency of the normal mode i. Each single pair of conjugated variables $\mathbf{Q}_i$ and $\mathbf{P}_i$ satisfies the probability given in eq 20, which results in a two-dimensional Gaussian distribution in the ($\mathbf{Q}_i$,$\mathbf{P}_i$) space. This provides us a way to perform the initial sampling of the coordinate and momentum for a chosen normal mode. This procedure will be repeated for each normal mode, and finally, the coordinates and momenta are converted back to Cartesian coordinates. Although eq 20 only gives the Wigner distribution of the vibrational ground level (at zero temperature), it is also possible to derive the Wigner distribution of a vibrational mode at a finite temperature.[143−146] Thus, in JADE, the initial coordinates and momenta can be sampled by the Wigner distribution for the quantum harmonic oscillator at zero or finite temperature. The initial sampling is not provided for vibrationally excited levels because of the possible negative probability of the Wigner function.[147,148]

Alternatively, the initial conditions for the nuclear coordinates and momenta can be obtained from classical action-angle variables[149] by assigning random values to the ($\mathbf{Q}_i$,$\mathbf{P}_i$) pairs corresponding to each of the dimensionless normal modes according to the following probability.

$$\mathbf{Q}_i = \sqrt{2n_i + 1}\,\sin\alpha_i \tag{21}$$

$$\mathbf{P}_i = \sqrt{2n_i + 1}\,\cos\alpha_i \tag{22}$$

where the angles α_i are randomly picked from the interval $[0,2\pi]$. The n_i corresponds to the quantum numbers of a harmonic oscillator. Further discussion of the dimensionless normal model is given in the Supporting Information. Moreover, a ($\mathbf{Q}_i$,$\mathbf{P}_i$) pair is given in terms of each normal mode and associated momentum. This procedure is repeated for each normal mode; then, the normal coordinates and momenta are converted back to Cartesian coordinates. In the JADE program, this sampling method is possible for a specific vibrational level n_i or at a finite temperature according to the Boltzmann distribution.

Currently, the harmonic frequencies and normal modes from the Turbomole, Gamess (US), and Gaussian packages have been interfaced. Additionally, in the sampling procedure, some normal modes, usually the low-frequency ones, can be "frozen" at their equilibrium values, with zero momenta. In the JADE package, the initial sampling of other regions of the configuration space beyond the Franck−Condon region is also possible, i.e., for dynamics simulations starting at a transition state (TS).[150−152] This sampling procedure generates a set of structures whose coordinates and momenta occupy the TS dividing surface at finite temperature. For large systems, a normal-mode analysis is not feasible, and a classical ground-state trajectory simulation can be used as an alternative to the probabilistic sampling of the initial conditions.

When a ground-state distribution is obtained from the sampling method, one needs to project this distribution onto the initial excited state. The simplest way to do this is to take all the initial conditions and vertically assign them to the excited state (Condon approximation). Further refinement is possible by filtering these geometries by their transition probability. On the basis of each sample configuration, the probability (p_{k0}) of an optical transition from the ground state S_0 to the excited state S_k is defined as

$$p_{k0} = \frac{f_{k0}/\omega_{k0}}{\max(f_{k0}/\omega_{k0})} \tag{23}$$

where f_{k0} is the oscillator strength and ω_{k0} is the energy difference between two states. Then, a stochastic procedure is

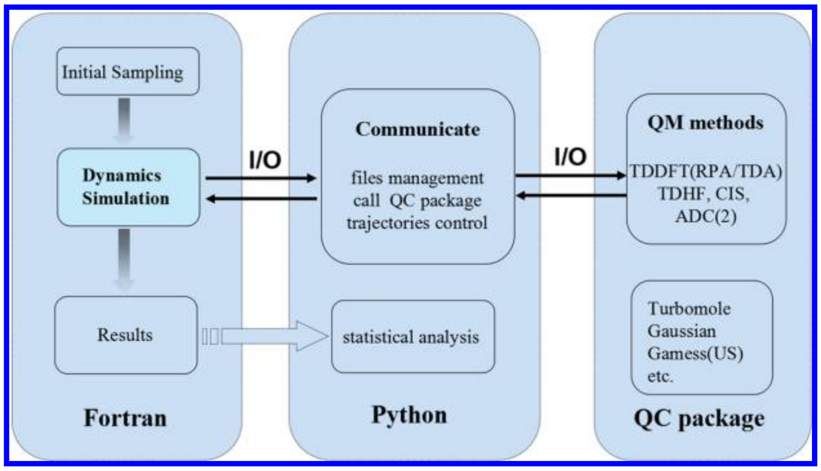

Figure 1. Basic code structure of the JADE program.

implemented to select or reject a given configuration by comparing the probability (p_{k0}) with a uniform random number.

2.5. Implementation and Technical Details. Currently, the JADE package is primarily used for the simulation of ultrafast nonadiabatic processes (femtosecond to picosecond time scale) in polyatomic molecules. The TSH dynamics are performed in an "on-the-fly" manner. Moreover, electronic structure calculations are required at each time step, which is much more time-consuming than the propagation of nuclear and electronic motions. For this purpose, we implemented the "on-the-fly" TSH dynamics for several single-reference electronic structure methods, such as CIS, TDHF, TDDFT (RPA and TDA), and ADC(2), which is cost-effective for medium- to large-sized systems. In principle, other excited-state methods can also be easily incorporated.

The basic code structure of the JADE package is organized in a modular way (Figure 1) by employing two computer languages, Fortran and Python. The Fortran code is used to do the basic and time-critical numerical calculations, such as dynamics propagation, numerical NAC, etc. The modification of this part is not necessary for users unless new dynamics algorithms are involved. Python is used to manage the input and output files and to communicate between the QC package and the dynamics module. The JADE program has been interfaced to several QC packages, i.e., Turbomole, Gaussian, and Gamess (US). Each code has a corresponding interface module in the JADE program, mostly written in Python to allow for extensions and to support additional features in external packages. The Python part can be easily modified for specific needs or to add new interfaces. The keywords for the dynamics in JADE are organized with a Fortran *namelist* and are supported by Fortran and Python modules. The basic input consists of a set of files defining the surface-hopping options and other data (initial coordinates and momenta, etc.). Additionally, an input template for the third-party package (i.e., Turbomole, Gaussian, Gamess (US) etc.) is required to perform the electronic structure calculations.

The general JADE workflow and analysis can be arranged in a few steps: (1) preparation of the initial conditions for dynamics simulations, (2) setup of the surface-hopping options and templates for electronic structure calculations, (3) postprocessing of the basic input for each trajectory, (4) execution of the dynamics simulation within the JADE program for sufficient time so that properties/phenomena of interest can be observed, and (5) statistical analysis of the dynamics results. Additional information is stored at each step (e.g., transition dipole moments) for further analysis. Various statistical tools are available in JADE, which is especially designed to consider multiple independent trajectories and which is mainly written in Python. Restart options are available to extend a completed trajectory or recover a crashed trajectory. Additionally, the LD thermostat is available to treat the dissipative dynamics. The JADE package is now publicly available (see details in the Supporting Information).

3. MODELS AND APPLICATIONS

In this section, we try to display various features of our package by discussing the excited-state dynamics simulations of several molecular systems. The current set of benchmark examples (Table 1) consists of the methaniminium cation ($CH_2NH_2^+$), fullerene (C_{20}), p-dimethylaminobenzonitrile (DMABN) and its primary amino derivative aminobenzonitrile (ABN), and 10-hydroxybenzo[h]quinoline (10-HBQ).

Table 1. TSH Investigations of Different Classes of Molecular Photoinduced Processes[a]

system	method	package	isolated	Langevin
$CH_2NH_2^+$	B3LYP	Gaussian	Y	Y
		Turbomole	Y	Y
	CAM-B3LYP	Gamess (US)	Y	Y
$CH_2NH_2^+{\cdot}3H_2O$	CAM-B3LYP	Gaussian	Y	Y
C_{20}	B3LYP	Gaussian	Y	Y
DMABN	CAM-B3LYP	Gaussian	Y	—
ABN	CAM-B3LYP	Gaussian	Y	—
10-HBQ	CAM-B3LYP	Gaussian	Y	—
	ADC(2)	Turbomole	Y	—

[a] Y, dynamics result available; —, dynamics calculation not performed.

In these simulations, the initial geometries and velocities of the nonadiabatic dynamics simulations were generated from the Wigner distribution function of the first vibrational level of the electronic ground state; although in principle other initial sampling methods are also supported by our package. The decoherence correction by Granucci and Persico was used, and the parameter was set to $\alpha = 0.1$ hartree.[153] Most calculations were performed at the TDDFT level. The ADC(2) level was employed for an excited-state intramolecular proton transfer (ESIPT) reaction of the 10-HBQ molecule. The nonadiabatic

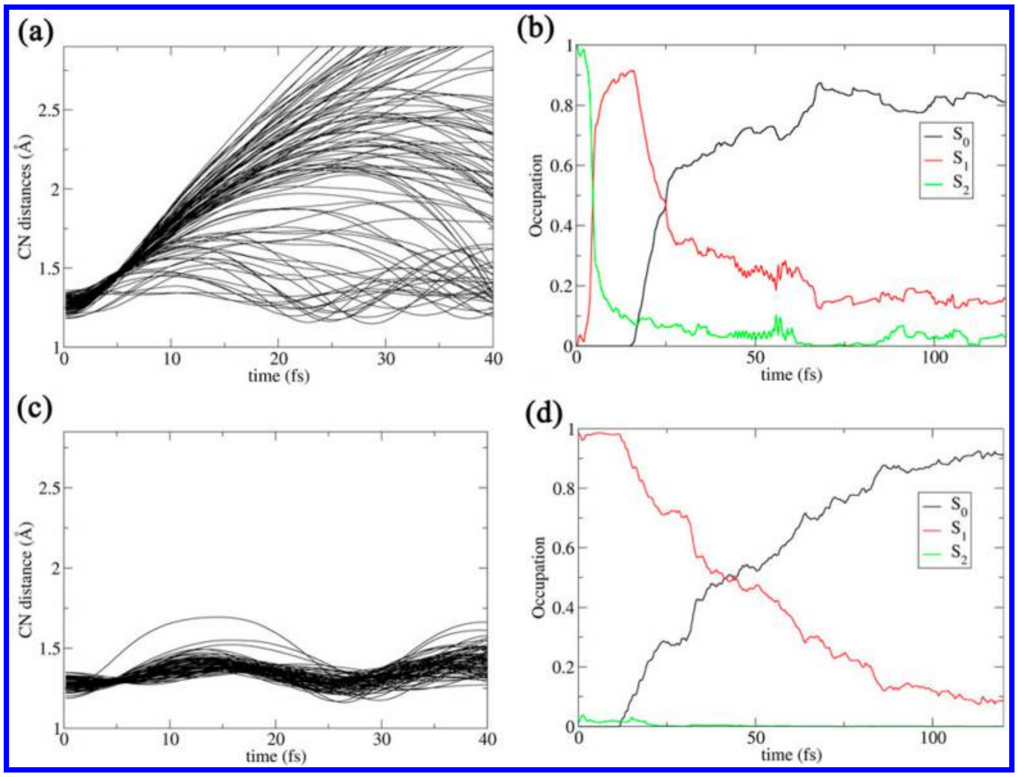

Figure 2. (a) CN stretching of the $CH_2NH_2^+$ molecule and (b) average fraction of trajectories for each state starting at the S_2 state. (c) CN stretching of the $CH_2NH_2^+$ molecule and (d) average fraction of trajectories for each state starting at the S_1 state.

dynamics of the $CH_2NH_2^+$, $CH_2NH_2^+\cdot 3H_2O$, and C_{20} molecules in an implicit environment are also investigated by LD simulations. In the LD simulations, different friction values (γ = 1, 50, and 100 ps^{-1}) were considered. The friction value[154] is related to the viscosity and particle size of the solvent and is used to mimic the viscosity properties of different solvents. For example, the value of 50 ps^{-1} is close to the viscosity of water molecules.[87,140] The friction constant for water molecules is also usually set to 62 ps^{-1} in LD simulations.[140,155,156]

3.1. Photoinduced Relaxation of the Methaniminium Cation ($CH_2NH_2^+$).

As a first application, we studied the photoinduced relaxation process of the methaniminium cation ($CH_2NH_2^+$), the smallest model mimicking retinal (rhodopsin chromophore). Due to its simplicity, the $CH_2NH_2^+$ molecule is usually a good candidate to test different methodologies.[125,157−159] The aim of this study is to test the implemented schemes and assess the quality of our results against available data from high-level methods.

The lifetimes along the average trajectories are calculated by exponential fitting to a function of the following form:[99]

$$f(t) = \exp(-t/\tau) \tag{24}$$

and the double exponential function decay model

$$f(t) = \frac{\tau_1}{\tau_2 - \tau_1}\left[\exp\left(\frac{t}{\tau_2}\right) - \exp\left(\frac{t}{\tau_1}\right)\right] \tag{25}$$

3.1.1. The Isolated System. The TSH dynamics for the isolated $CH_2NH_2^+$ molecule was performed in the framework of the JADE package. The nuclear equations of motion were integrated with a time step of 0.2 fs, and the electronic amplitude was propagated with a time step of 0.002 fs. The results were obtained by averaging 100 trajectories. The electronic structure calculations for $CH_2NH_2^+$ have been performed at the TDDFT-B3LYP/6-31G** level with the Turbomole, Gaussian, and Gamess (US) packages. The dynamics simulations with the different electronic structure packages were consistent with each other, and thus, only the results from Gaussian are reported.

After the initial sampling on the ground state, the system is vertically excited onto the $\pi-\pi^*$ state (S_2). Then, the system switches very rapidly from the S_2 state to the S_1 state through the S_1/S_2 conical intersection. As shown in Figure 2a, the trajectories mainly split in two branches in terms of the evolution of the CN distance within the first 10 fs. One branch displays the strong excitation of the CN stretching mode, yielding the weakly bound $CH_2^+\cdots NH_2$ complex, while in the other branch, the CN bond length remains relatively short and shows a weak oscillation (less than 1.6 Å). This behavior was also reported in the TSH dynamics at a high-level *ab initio* theory.[99,157] The average fraction of trajectories for each state is shown in Figure 2b. The $S_2 \rightarrow S_1$ hops occur during the first 10 fs, after which the relaxation continues on the S_1 state. The lifetime of S_2 is estimated to be approximately 8 ± 1 fs, similar to the ~10 fs calculated at the CASSCF level[157] or ~12 fs calculated at the MR-CISD level.[99] Most of the trajectories jump back to the ground state within 30−100 fs. All the above results also agree well with previous TSH dynamics simulations on the $CH_2NH_2^+$ molecule at the TDDFT-PBE level.[125]

The dynamics behavior of $CH_2NH_2^+$ starting on the S_1 state is rather different. As shown in Figure 2c, the splitting of the trajectories starting on the S_1 state is very rare, and most of the CN bonds remain relatively short (~1.2−1.4 Å). The weak CN stretching mode has also been previously observed at the MR-CISD level.[99] An exponential decay of the S_1 state is observed after the first 10 fs (Figure 2d). The reverse hops to the S_2 state

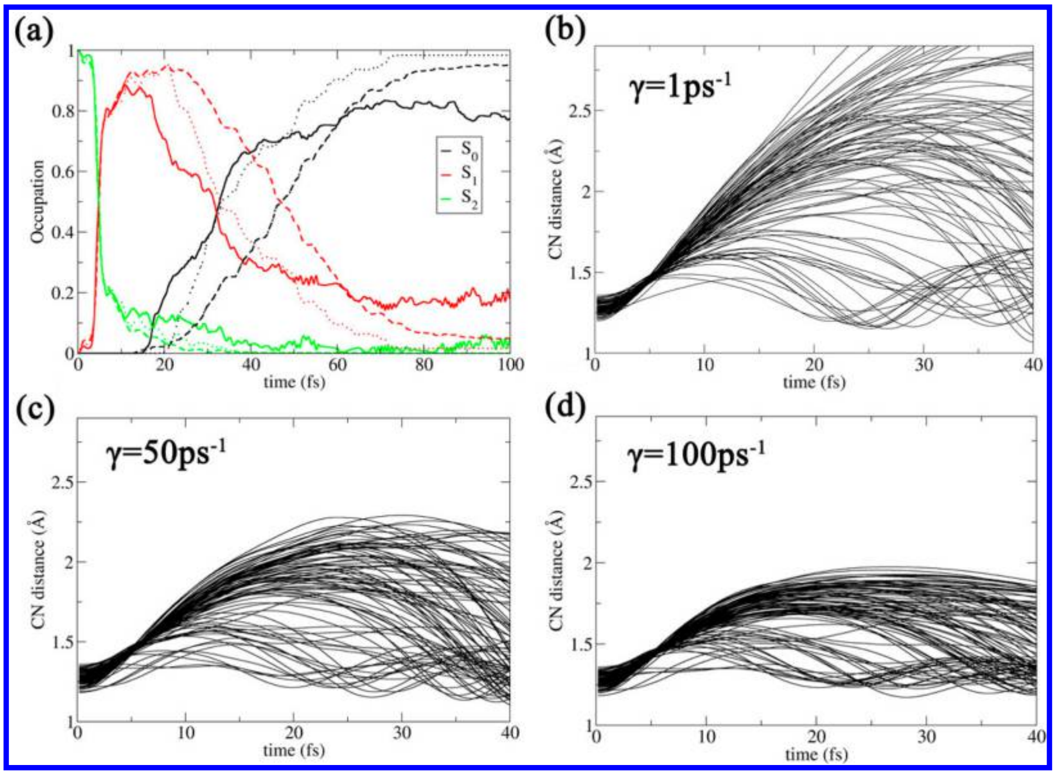

Figure 3. (a) Average fraction of trajectories for the $CH_2NH_2^+$molecule with the LD scheme with friction γ = 1 (straight line), 50 (dotted line), and 100 (dashed line) ps^{-1}. The CN stretching of the $CH_2NH_2^+$ as a function of time (fs) for (b) γ = 1, (c) γ = 50, and (d) γ = 100 ps^{-1}.

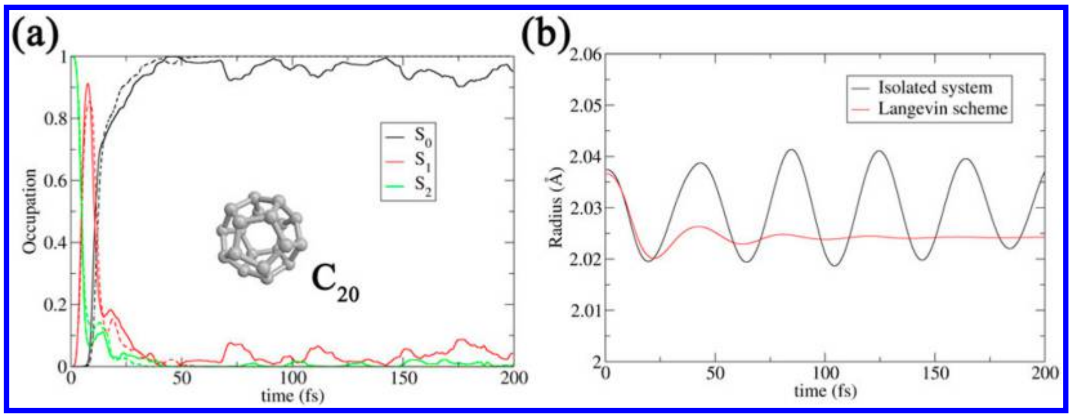

Figure 4. (a) Average fraction of trajectories for each state as a function of time (fs) for isolated systems (solid line) and Langevin dynamics (dashed line). (b) The average radius of a C_{20} molecule as a function of time (fs).

often occur in the initial stage of the dynamics starting on the S_1 state. The S_1lifetime was estimated to be ~65 fs, which is comparable to the result (~69 fs) obtained at the MR-CISD level.[99]

We also tried to examine the influence of several setup parameters of the electronic structure calculations on the dynamics, i.e., Casida's assignment ansatz, the output accuracy of the electronic structure calculations, and the effects of functionals. Most of these results are collected in the Supporting Information. In summary, for the above numerical simulations, the nonadiabatic dynamics at the TDDFT level with different setups were in good agreement with the ones computed at high *ab initio* levels, both from a qualitative and quantitative point of view. However, relative differences were also observed, i.e., with the range-separated functional CAM-B3LYP, the population decay seems to be slower in the excited states (Figure S2b). Additionally, although a deficiency in the PES topology in the vicinity of the S_0/S_1 conical intersection exists at the TDDFT level,[58,64−66,136,138,160] the promising numerical results of the current nonadiabatic dynamics seems to provide an approximated description of the $S_1 \rightarrow S_0$ decay dynamics, at least qualitatively.

3.1.2. Langevin Dynamics Simulation. Here, the nonadiabatic dynamics of the $CH_2NH_2^+$ molecule with environment effects is also investigated by LD simulations. Also starting from the S_2 state, the TSH dynamics simulations (for 100 trajectories) were performed at the TDDFT-B3LYP/6-31G** level within the Gaussian 09 package. The time step of the nuclear motion was 0.2 fs, and the electronic amplitude was propagated with a time step of 0.002 fs. Several friction values (γ = 1, 50, 100 ps^{-1}) were used, and the temperature was set to 300 K. Additionally, the simulations of $CH_2NH_2^+$ with a few

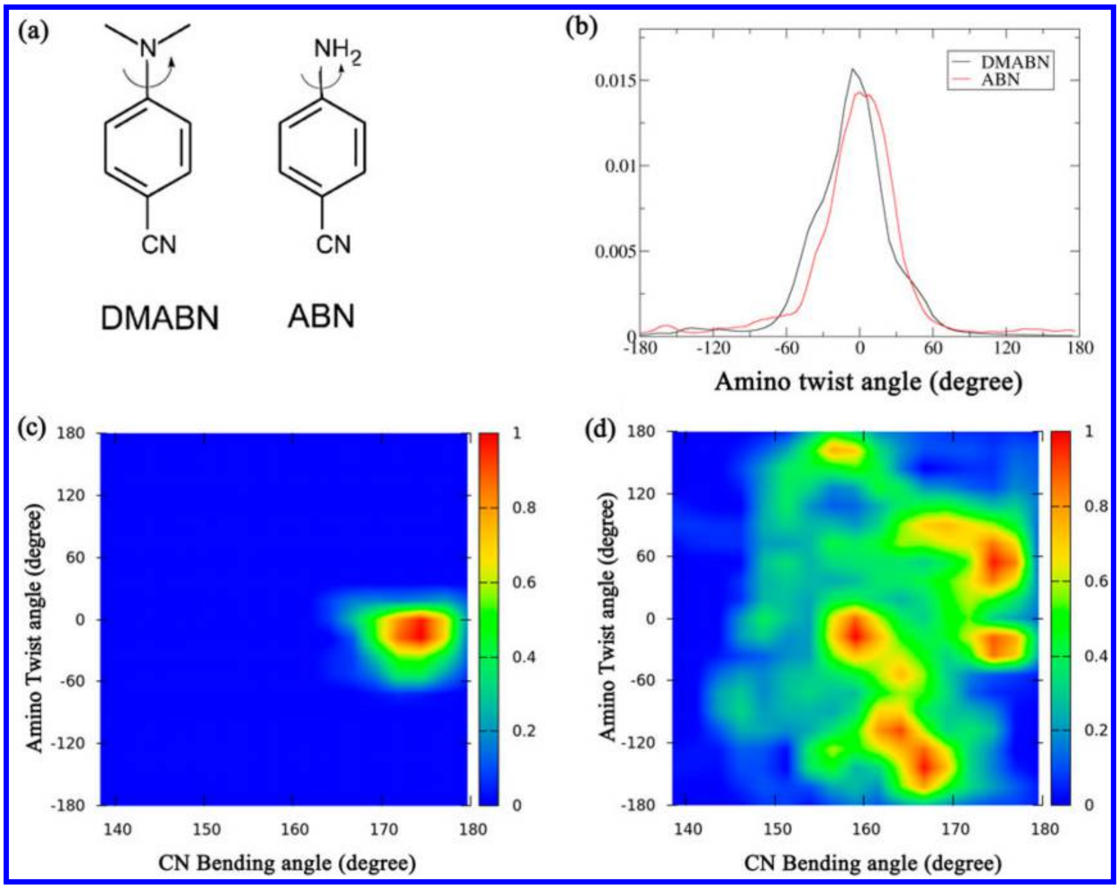

Figure 5. (a) Structures of DMABN and ABN. (b) Amino twist angle distribution for the $S_2 \rightarrow S_1$hopping events for the DMABN and ABN molecule; two-dimensional geometric distribution of the twist angle and $-C{\equiv}N$ bending angle along the propagation of a typical trajectory for (c) DMABN and (d) ABN.

explicit water molecules ($CH_2NH_2^+ \cdot 3H_2O$) were also examined and are summarized in the Supporting Information.

As shown in Figure 3a, the average fractional occupations of the trajectories for three different friction values γ were similar to each other for the first 10 fs, implying that the environmental friction does not affect the extremely fast decay process. Thus, the lifetime (~10 fs) of the S_2 state is only slightly affected by the friction (γ) and is very close to that of the isolated system. However, the friction effect becomes apparent for the dynamics on the S_1 state, leading to a slower decay. Interestingly, the LD simulations completely modify the molecular motion. As shown in Figure 3, when the friction γ is small (1 ps^{-1}), the evolution of the CN bond is similar to that of the isolated system. However, if the friction γ increases to 50 or 100 ps^{-1}, the CN bond stretching motion is highly suppressed by the damping effects caused by friction; thus, the bond cleavage is dramatically reduced.

3.2. Fullerene (C_{20}). Fullerenes are known to be excellent electron acceptors in photovoltaic materials due to their unique π-electron properties.[161] Here, the TSH dynamics were performed for a relatively small fullerene molecule (C_{20}) at the TDDFT-B3LYP/6-31G* level, interfaced with the Gaussian 09 package. The time step was set to be 0.5 fs, while the electronic motion was propagated with a time step of 0.005 fs. Starting from the initial sampling geometries of the ground state, the C_{20} was electronically excited to the S_2 state. For comparison, the LD scheme was also applied with γ = 50 ps^{-1} and T = 300 K.

As shown in Figure 4a, the C_{20} molecule exhibits an extremely fast decay of its excited states, and the lifetime of the S_1 and S_2 states is estimated to be approximately 5.8 and 9.2 fs, respectively. After the first 20 fs, the occupation of the ground state dominates (>90%), and the nonadiabatic dynamics is essentially over. The LD simulations provide similar decay trends of the occupation, possibly because the current decay is too fast (only a few fs) to be modified by the fluctuations of the thermal bath. Another interesting result is the periodical motion (~40 fs) of the radius of the C_{20} molecule (Figure 4b). After the LD scheme was applied, such oscillations of the radius were largely suppressed and disappeared very quickly due to the vibrational relaxation caused by the friction of the environment. During both dynamics simulations (either of the isolated system or with the LD scheme), the breaking of the C−C bond was not observed. Additionally, the similar relaxation behavior of the isolated C_{20} molecule starting from the S_3 state was also observed, which is summarized in Figure S4 of the Supporting Information. The observed relaxation mode has also been reported in a few fullerenes systems on the basis of experimental Raman spectra or computational studies.[162,163] Thus, these results may be a common phenomenon in the excited-state motion of fullerenes. However, further work is required to provide more detailed understanding of these phenomena.

3.3. DMABN/ABN Molecules. The dual luminescence of p-dimethylaminobenzonitrile (DMABN) and its derivatives were reported by Lippert et al. in the early 1960s.[164] When these molecules are excited in the near UV region, two possible

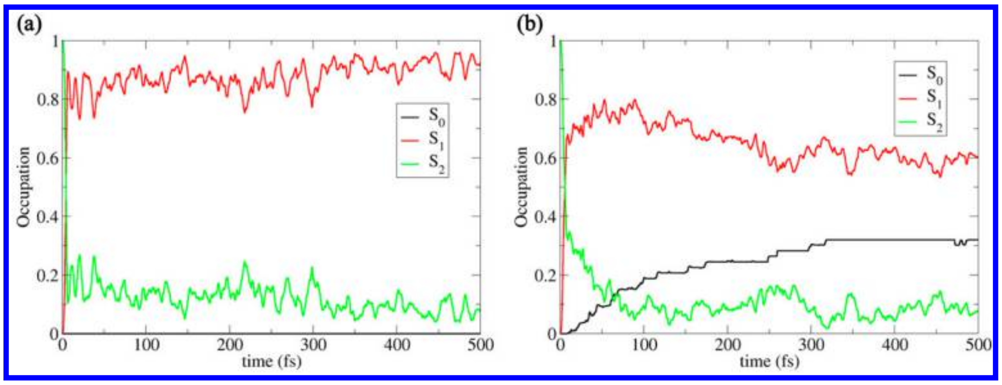

Figure 6. Average fraction of trajectories for each state as a function of time (fs) for (a) DMABN and (b) ABN.

fluorescence bands can be observed: one with the a usual small Stokes shift (attributed to a benzenoid π–π^* excited state, a locally excited (LE) state) and a second band with a large red shift (attributed to the emission from a highly polar intramolecular charge-transfer (ICT) state). Dual fluorescence is usually dependent on the relative energy of the two states, which can be fine-tuned by the environments, such as the polarity of the solvent. This phenomenon is widely applied in many fields, including laser dyes, biological and chemical fluorescence detectors, molecular switching devices, solar energy utilization, etc.[165−170] However, its primary amino derivative, aminobenzonitrile (ABN), does not show dual fluorescence even in a highly polar solvent.[171] There have been controversial discussions over the existence of twisted induced intramolecular charge-transfer (TICT) and planar ICT states.[168,171−175] For electron donor/acceptor species such as DMABN, the excitation to the S_2 state is followed by the $S_2 \rightarrow S_1$ internal conversion. Experimental evidence[176,178] also confirmed that the evolution of the excited state S_2 is followed by an ultrafast internal conversion to the S_1 state and a subsequent evolution to the LE and ICT minimum energy structures. Therefore, the initial stage of the reaction path ($S_2 \rightarrow S_1$ relaxation) after light absorption must be nonadiabatic. Thus, one of the central issues is to understand the nonadiabatic reaction occurring via a S_2/S_1 conical intersection (CI) and connecting the FC structure on S_2 to the species of the S_1 state.

In this work, the TSH dynamics simulations were performed to characterize the $S_2 \rightarrow S_1$ deactivation channel for DMABN and ABN (Figure 5a), in which the Wigner sampling was employed and S_2 was the initial electronic state. The DMABN and ABN molecules contain both electron donating ($-N(CH_3)_2$ or $-NH_2$) and accepting ($-CN$) groups, and hence, the charge transfer effect is critical in the excited-state dynamics. Thus, the range-separated functional CAM-B3LYP/6-31G* in Gaussian was adopted. The simulations were performed for 50 trajectories with a time step of 0.5 fs, while the electronic motion was propagated with a time step of 0.005 fs. The presented results also aim at clarifying some controversial aspects associated with electron donor/acceptor TICT processes.

As shown in Figure 5b, the distribution of the amino twist dihedral angles during the $S_2 \rightarrow S_1$ hopping events indicates that planar geometries with an untwisted amino group is preferred at the crossing points (S_2/S_1); however, the slightly twisted geometries are also possible. This is consistent with the analysis of the conical intersection seam at the CASSCF level,[177] which also indicates that the $S_2 \rightarrow S_1$ internal conversion does not require the amino group twist because the seam is accessible for a large range of torsional angles. Note that the DMABN molecule shows slightly sharper distribution behaviors than ABN molecules, which can be rationalized on the basis of the larger $-N(CH_3)_2$ group present in DMABN. Furthermore, the motion of an electron acceptor ($-C{\equiv}N$) in the *para* position is also important.[178] A typical trajectory (1000 fs) was selected to study the correlation between the amino twist angle and the cyano group ($-C{\equiv}N$) bending motion with time (Figure 5c,d). The internal rotation of the dimethylamino group in DMABN is observed although the planar structure is preferred on the simulation time scale. For the ABN molecules, the system relaxation can take place at various torsional angles of the dimethylamino group, and the trajectory seems to go back and forth between different minima on the PES. This indicates that the dynamics of DMABN and ABM are remarkably different.

Figure 6 provides the average fraction of trajectories for each state. For the comparison with experimental observations, we initially suppose that the decay process is composed of several time scales, and the molecule sequentially reaches several locations on the PES. For DMABN, the initial quick drop of S_2 state population is observed within 10 fs, and estimated lifetime (τ_1) is about 5.9 ± 1 fs. This ultrafast step indicates that the system quickly leaves the Franck−Condon (FC) region along active higher-frequency vibration modes to access the S_2/S_1 conical intersection. Then, the continuous decay (20% to 10%) of the S_2 state is observed along with fast oscillations, while such decay stops at around 150 fs with an estimated lifetime (τ_2) of 80 ± 15 fs. After it, the weaker recurrence with much longer time-scale dynamics seems to exist. The two ultrafast decay time constants were consistent with the experimental findings ($\tau_1 = 5 \pm 5$ fs and $\tau_2 = 63 \pm 5$ fs).[178] The assignment of different decay time scales of ABN molecule is more transparent. The early state of the S_2 state decay clearly gives two time scales ($\tau_1 = 12 \pm 1$ fs and $\tau_2 = 40 \pm 3$ fs), which are also consistent with the experimental observations ($\tau_1 = 15 \pm 5$ fs and $\tau_2 = 35 \pm 5$ fs) of ABN.[178] For both DMABN and ABN molecules, we found that the completed decay of the S_2 state is below 100 fs ($\tau_1 + \tau_2$). Later on, the occupation of the ground state S_0 state is negligible for DMABN, while the population of the S_0 state is observed for ABN during the first 500 fs. This indicates that the S_0/S_1 conical intersection is more accessible for ABN than for DMABN, which may arise from the more flexible $-NH_2$ group present in ABN compared to the $-N(CH_3)_2$ group present in DMABN. This may explain why the dual luminescence is not observed for the ABN molecule in the experiments.

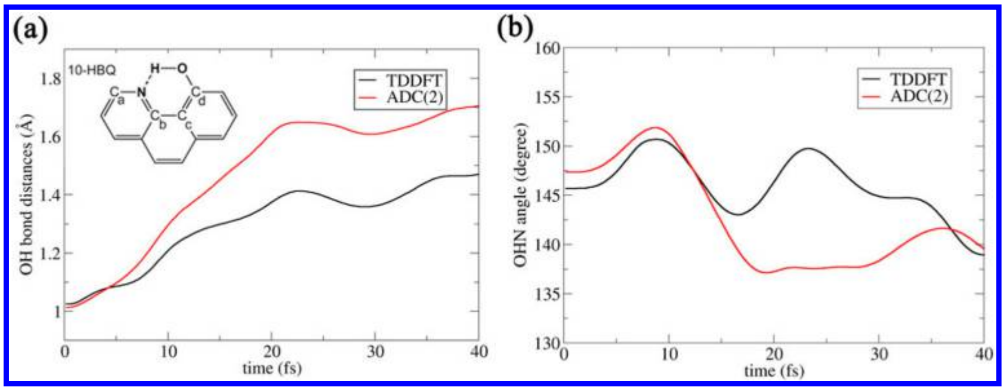

Figure 7. Time evolution of (a) the OH distance and (b) ∠OHN averaged over all the trajectories for 10-HBQ at the TDDFT and ADC(2) levels.

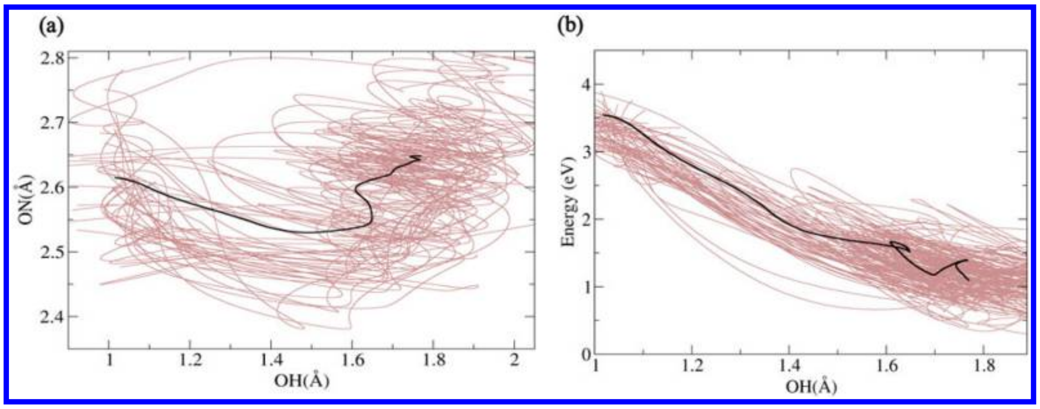

Figure 8. (1) Geometric correlation between the OH and ON distances at the ADC(2) level. (2) S_1−S_0 energy gap as a function of the OH distance at the ADC(2) level. The black line represents the evolution of the average trajectory, and the gray line represents the propagation of each trajectory.

3.4. Excited-State Intramolecular Proton Transfer of 10-HBQ.

Intramolecular proton transfers in excited states (ESIPT) are extensively studied to gain insight into fundamental photophysical and photochemical processes.[11,179−186] Comprehensive experimental and theoretical investigations have been performed on several compounds such as HBT (2-(2′-hydroxyphenyl)-benzothiazole)[187−189] and 10-HBQ (10-hydroxybenzo[h]quinoline).[184,185,190,191] Here, the 10-HBQ molecule is adopted as a model system to study the ultrafast ESIPT process. The initial conditions for each trajectory were generated by the Wigner sampling approach, and the molecule was then excited to the first singlet excited state (S_1). The dynamics simulations were performed with two theoretical methods: (1) at the ADC(2)/def2-SVP level within the Turbomole package; (2) at the TDDFT-CAM-B3LYP/6-31G** level within the Gaussian 09 package. The simulations were performed for 50 trajectories with a time step of 0.2 fs.

The 10-HBQ molecule has an intramolecular hydrogen bond (Figure 7a). In the electronic ground state, the enolform with the hydrogen atom bound to the donor oxygen of the H-chelate ring is the stable tautomer, and the hydrogen atom of the hydroxyl group is transferred to the nitrogen at the opposite side of the ring after photoexcitation to the first excited state (S_1). The excited-state tautomer is rapidly formed within the first 20 fs, identified by the longer and more stable OH distance (Figure 7a). The TDDFT and ADC(2) methods predicted the very close ESIPT rate. However, the ADC(2) method predicted a larger OH distance, and this can be rationalized by the time evolution of ∠OHN (Figure 7b), in which the ∠OHN angle at the ADC(2) level decays to a lower value (∼140°) after approximately 20 fs. The estimated ESIPT rate (∼20 fs) at both the ADC(2) and TDDFT levels is consistent with the reported ESIPT rate of 10-HBQ by Lee et al. (12 ± 6 fs),[192] Higashi and Saito (29 fs),[193] and Kim and Joo (13 fs).[194] Overall, the dynamics simulations confirmed the ultrashort time scale of the ESIPT in 10-HBQ[189] and provided a detailed picture of the structural aspects of that process.

The skeletal motions in 10-HBQ have been proposed to be responsible for the ESIPT process,[195] where the role of the proton in ESIPT may be active, passive, or semipassive. Different mechanisms have been proposed to understand the role of the proton.[185,193−195] Here, we performed an analysis of the time evolution of the ON and OH distances at the ADC(2) level. The results from the averaged trajectory indicate that the proton transfer process takes place in a few steps. At first, the proton transfer starts with an OH-bond elongation and an ON distance shortening, and then the OH distance increased while the ON distance remained almost constant. Further into the simulation, the ON distance increased again, after which the transfer was complete. This conclusion seems to be available for most of the trajectories. Thus, the role of the proton may be considered semipassive for the HBQ molecule.[185,195] When the proton transfer was completed, the average energy gap of the S_1/S_0 energy gap decreased from 3.6 to 1.1 eV (Figure 8b), which may facilitate the subsequent internal conversion.[189]

4. CONCLUSIONS

In this report, the JADE program, designed as a general-purpose code for direct surface-hopping dynamics simulations based on Tully's fewest-switches algorithm, is introduced. As an important extension to the classical treatment of nuclear motion, the LD scheme was implemented to mimic the environment effects. Currently, several electronic structure methods (CIS, TDHF, TDDFT (RPA and TDA), and ADC(2)) are supported, especially the TDDFT method, aiming at performing nonadiabatic dynamics simulations for medium- to large-sized molecules, such as amino acids and transition metal complexes. Basic statistical tools for post-processing the dynamics results are available in JADE. They can provide averages and standard deviations over trajectories as a function of time for various quantities. In addition, the initial sampling code, which is able to produce the proper geometries and momentum distributions with various sampling technologies, is also available. This provides us with means to perform sampling, such as at different temperatures and in specific regions of the potential energy surface. The modularity of the JADE code allows the possible incorporation of other trajectory-based methods (i.e., the Ehrenfest approach). Currently, the JADE program has been interfaced to several QC packages, i.e., Turbomole, Gaussian, and Gamess (US). Because the dynamics code is loosely linked to the QC package, the incorporation of other QC packages is very straightforward.

The excited-state dynamics simulations of various model systems were performed to illustrate several features of the JADE package. The deactivation path of the $CH_2NH_2^+$ molecule was studied as a benchmark system. The results presented similar features compared with available MRCI or CASSCF results. The different implementations of nonadiabatic coupling term calculations and the dependence of the output accuracy of the QC package were evaluated, and similar results were reproduced in the TSH dynamics simulations. The choice of density functional seems to have potential influences on the dynamics simulations results. For the fullerene (C_{20}), the ultrafast breathing motion of the radius is discussed in the nonadiabatic dynamics simulations starting from excited states. The nonadiabatic dynamics of DMABN/ABN molecules was discussed, and the differences, including structural evolution and excited-state population, are addressed. The dynamics simulations of 10-HBQ confirmed the ultrashort time scale of the ESIPT in 10-HBQ[189] and indicated the semipassive role of the skeletal motions. Furthermore, the LD scheme was applied in the simulation of the $CH_2NH_2^+$ cation and the fullerene (C_{20}) molecule. The frictions show a small influence on short-time decay dynamics but obvious effects on the long-time dynamics. The weak and strong frictions of the environment are compared, and the strong frictions significantly modify the evolution of the geometry in the dynamics simulations. The simulations of $CH_2NH_2^+$ with explicit water molecules also provided rich information about the features and limitations of the LD scheme. In summary, the LD scheme provides an easy-to-use mean to investigate photoinduced reactions in complex systems.

We hope that the developed computational package will motivate further developments of more advanced and state-of-the-art on-the-fly dynamics methods and facilitate future studies in the field of photochemistry and related disciplines. Further work is also ongoing to incorporate the spin-flip TDDFT method,[196,197] which seems to be a promising approach to treat the S_0/S_1 conical intersection.[197,198] The work on the interface with the semiempirical program MNDO, and with Q-CHEM and Molpro, is in progress. The incorporation of a hybrid method (QM/MM) with polarizable force fields to address complex systems is an interesting subject for future studies. Another challenging issue is the inclusion of spin−orbit coupling effects. Certainly, the combination of more rigorous semiclassical dynamics with "on-the-fly" approaches represents a great challenge for the future. We believe that all of these possible extensions will bring new features in the JADE code and will allow us to study different types of photoinduced dynamics in various complex systems.

■ ASSOCIATED CONTENT

Ⓢ Supporting Information

Details about the JADE package, technical details of NAC couplings at the TDDFT level, examination of setup parameters in the electronic structure calculations, photoinduced relaxation of the $CH_2NH_2^+{\cdot}3H_2O$ complex, and the isolated C_{20} system starting from the S_3 state. This material is available free of charge via the Internet at http://pubs.acs.org.

■ AUTHOR INFORMATION

Corresponding Author

*Fax: +86-532-80662778. Tel.: +86-532-80662630. E-mail: lanzg@qibebt.ac.cn.

Author Contributions

The manuscript was written with the contributions of all the authors. All authors have given approval to the final version of the manuscript.

Notes

The authors declare no competing financial interest.

■ ACKNOWLEDGMENTS

The authors wish to thank Dr. Yu Xie who assisted in the proofreading of the manuscript. This work is supported by the CAS 100 Talent Project, NSFC project (Grant No. 21103213 and 91233106). The authors thank the Supercomputing Center, Computer Network Information Center (Beijing), CAS, and the Super Computational Center of CAS-QIBEBT for computational resources and software. The authors also thank the support by (Grant No. 14HZ03) the Key Lab of Nanodevices and Nanoapplications, Suzhou Institute of Nano-Tech and Nano-Bionics, CAS.

■ REFERENCES

(1) Piotrowiak, P. *Chem. Soc. Rev.* **1999**, *28*, 143−150.

(2) Shukla, M., Leszczynski, J. Radiation Induced Molecular Phenomena In Nucleic Acids: A Brief Introduction. In *Radiation Induced Molecular Phenomena in Nucleic Acids: A Comprehensive Theoretical and Experimental Analysis*; Springer Verlag: Berlin, 2008; pp 1−14.

(3) Yarkony, D. R. *Chem. Rev.* **2011**, *112*, 481−498.

(4) Domcke, W.; Yarkony, D. R. *Annu. Rev. Phys. Chem.* **2012**, *63*, 325−352.

(5) Yarkony, D. R. Conical Intersections: Their Description and Consequences. In *Conical Intersections:Theory, Computation and Experiment*; Wolfgang Domcke, D. R. Y., Köppel, H., Eds.; World Scientific: 2004; pp 41−128.

(6) Nakamura, H., Introduction: What is "Nonadiabatic Transition"? In *Nonadiabatic Transition: Concepts, Basic Theories and Applications*; World Scientific: 2012; pp 1−5.

(7) Plasser, F.; Barbatti, M.; Aquino, A. A.; Lischka, H. *Theor. Chem. Acc.* **2012**, *131*, 1−14.

(8) Barbatti, M.; Aquino, A. J. A.; Szymczak, J. J.; Nachtigallová, D.; Hobza, P.; Lischka, H. *Proc. Natl. Acad. Sci. U. S. A.* **2010**, 21453−21458.

(9) Chen, J.; Thazhathveetil, A. K.; Lewis, F. D.; Kohler, B. *J. Am. Chem. Soc.* **2013**, *135*, 10290−10293.

(10) Fron, E.; Sliwa, M.; Adam, V.; Michiels, J.; Rocha, S.; Dedecker, P.; Hofkens, J.; Mizuno, H. *Photochem. Photobiol. Sci.* **2014**, *13*, 867–874.

(11) Chattoraj, M.; King, B. A.; Bublitz, G. U.; Boxer, S. G. *Proc. Natl. Acad. Sci. U. S. A.* **1996**, *93*, 8362–8367.

(12) Corrales, M. E.; González Vázquez, J.; Balerdi, G.; Solá, I. R.; de Nalda, R.; Bañares, L. *Nat. Chem.* **2014**, *6*, 785–790.

(13) Tully, J. C. *J. Chem. Phys.* **1990**, *93*, 1061–1071.

(14) Bixon, M.; Jortner, J. *J. Chem. Phys.* **1968**, *48*, 715–726.

(15) Worth, G. A.; Hunt, P.; Robb, M. A. *J. Phys. Chem. A* **2003**, *107*, 621–631.

(16) van Harrevelt, R.; Manthe, U. *J. Chem. Phys.* **2005**, *123*, 064106.

(17) Meng, Q.; Meyer, H.-D. *J. Chem. Phys.* **2013**, *138*, 014313.

(18) Manthe, U. *J. Chem. Phys.* **2008**, *128*, 164116.

(19) Ben-Nun, M.; Quenneville, J.; Martínez, T. J. *J. Phys. Chem. A* **2000**, *104*, 5161–5175.

(20) Ben-Nun, M.; Martínez, T. J. *J. Chem. Phys.* **1998**, *108*, 7244–7257.

(21) Levine, B. G.; Coe, J. D.; Virshup, A. M.; Martínez, T. J. *Chem. Phys.* **2008**, *347*, 3–16.

(22) Horenko, I.; Salzmann, C.; Schmidt, B.; Schütte, C. *J. Chem. Phys.* **2002**, *117*, 11075–11088.

(23) Donoso, A.; Martens, C. C. *J. Phys. Chem. A* **1998**, *102*, 4291–4300.

(24) Burghardt, I.; Cederbaum, L. S. *J. Chem. Phys.* **2001**, *115*, 10312–10322.

(25) Curchod, B. F.; Tavernelli, I. *J. Chem. Phys.* **2013**, *138*, 184112.

(26) Wang, H.; Thoss, M.; Miller, W. H. *J. Chem. Phys.* **2000**, *112*, 47–55.

(27) Sun, X.; Miller, W. H. *J. Chem. Phys.* **1997**, *106*, 6346–6353.

(28) Miller, W. H. *J. Phys. Chem. A* **2001**, *105*, 2942–2955.

(29) Gerber, R. B.; Buch, V.; Ratner, M. A. *J. Chem. Phys.* **1982**, *77*, 3022–3030.

(30) Micha, D. A. *J. Chem. Phys.* **1983**, *78*, 7138–7145.

(31) Li, X.; Tully, J. C.; Schlegel, H. B.; Frisch, M. J. *J. Chem. Phys.* **2005**, *123*, 084106.

(32) Miller, W. H.; George, T. F. *J. Chem. Phys.* **1972**, *56*, 5637–5652.

(33) Bittner, E. R.; Rossky, P. J. *J. Chem. Phys.* **1995**, *103*, 8130–8143.

(34) Coker, D. F.; Xiao, L. *J. Chem. Phys.* **1995**, *102*, 496–510.

(35) Kuntz, P. J. *J. Chem. Phys.* **1991**, *95*, 141–155.

(36) Webster, F.; Wang, E. T.; Rossky, P. J.; Friesner, R. A. *J. Chem. Phys.* **1994**, *100*, 4835–4847.

(37) Prezhdo, O. V.; Rossky, P. J. *J. Chem. Phys.* **1997**, *107*, 825–834.

(38) Zhu, C.; Jasper, A. W.; Truhlar, D. G. *J. Chem. Phys.* **2004**, *120*, 5543–5557.

(39) Andersson, K.; Malmqvist, P. A.; Roos, B. O.; Sadlej, A. J.; Wolinski, K. *J. Phys. Chem.* **1990**, *94*, 5483–5488.

(40) Meissner, L. *Int. J. Quantum Chem.* **2008**, *108*, 2199–2210.

(41) González, L.; Escudero, D.; Serrano-Andrés, L. *ChemPhysChem* **2012**, *13*, 28–51.

(42) Eade, R. H. A.; Robb, M. A. *Chem. Phys. Lett.* **1981**, *83*, 362–368.

(43) Pulay, P. *Int. J. Quantum Chem.* **2011**, *111*, 3273–3279.

(44) Malmqvist, P. A.; Rendell, A.; Roos, B. O. *J. Phys. Chem.* **1990**, *94*, 5477–5482.

(45) Andersson, K.; Malmqvist, P. Å.; Roos, B. O. *J. Chem. Phys.* **1992**, *96*, 1218–1226.

(46) Lischka, H.; Shepard, R.; Pitzer, R. M.; Shavitt, I.; Dallos, M.; Muller, T.; Szalay, P. G.; Seth, M.; Kedziora, G. S.; Yabushita, S.; Zhang, Z. *Phys. Chem. Chem. Phys.* **2001**, *3*, 664–673.

(47) Silva-Junior, M. R.; Thiel, W. *J. Chem. Theory Comput.* **2010**, *6*, 1546–1564.

(48) Keal, T.; Koslowski, A.; Thiel, W. *Theor. Chem. Acc.* **2007**, *118*, 837–844.

(49) Weber, W.; Thiel, W. *Theor. Chem. Acc.* **2000**, *103*, 495–506.

(50) Strodel, P.; Tavan, P. *J. Chem. Phys.* **2002**, *117*, 4677–4683.

(51) Soler, M. A.; Roitberg, A. E.; Nelson, T.; Tretiak, S.; Fernandez-Alberti, S. *J. Phys. Chem. A* **2012**, *116*, 9802–9810.

(52) Dewar, M. J. S.; Zoebisch, E. G.; Healy, E. F.; Stewart, J. J. P. *J. Am. Chem. Soc.* **1985**, *107*, 3902–3909.

(53) Comeau, D. C.; Bartlett, R. J. *Chem. Phys. Lett.* **1993**, *207*, 414–423.

(54) Stanton, J. F.; Bartlett, R. J. *J. Chem. Phys.* **1993**, *98*, 7029–7039.

(55) Christiansen, O.; Koch, H.; Jørgensen, P. *Chem. Phys. Lett.* **1995**, *243*, 409–418.

(56) Rusakova, I. L.; Krivdin, L. B.; Rusakov, Y. Y.; Trofimov, A. B. *J. Chem. Phys.* **2012**, *137*, 044119.

(57) Trofimov, A. B.; Stelter, G.; Schirmer, J. *J. Chem. Phys.* **1999**, *111*, 9982–9999.

(58) Dreuw, A.; Head-Gordon, M. *Chem. Rev.* **2005**, *105*, 4009–4037.

(59) Gross, E. K. U.; Dobson, J. F.; Petersilka, M. Density functional theory of time-dependent phenomena. In *Density Functional Theory II*; Nalewajski, R. F., Ed.; Springer: Berlin, 1996; Vol. *181*, pp 81–172.

(60) Jamorski, C.; Casida, M. E.; Salahub, D. R. *J. Chem. Phys.* **1996**, *104*, 5134–5147.

(61) Parac, M.; Grimme, S. *J. Phys. Chem. A* **2002**, *106*, 6844–6850.

(62) Tozer, D. J.; Amos, R. D.; Handy, N. C.; Roos, B. O.; Serrano-Andres, L. *Mol. Phys.* **1999**, *97*, 859–868.

(63) Liu, W.; Settels, V.; Harbach, P. H. P.; Dreuw, A.; Fink, R. F.; Engels, B. *J. Comput. Chem.* **2011**, *32*, 1971–1981.

(64) Levine, B. G.; Ko, C.; Quenneville, J.; Martínez, T. J. *Mol. Phys.* **2006**, *104*, 1039–1051.

(65) Gozem, S.; Melaccio, F.; Valentini, A.; Filatov, M.; Huix-Rotllant, M.; Ferré, N.; Frutos, L. M.; Angeli, C.; Krylov, A. I.; Granovsky, A. A.; Lindh, R.; Olivucci, M. *J. Chem. Theory Comput.* **2014**, *10*, 3074–3084.

(66) Curchod, B. F. E.; Rothlisberger, U.; Tavernelli, I. *ChemPhysChem* **2013**, *14*, 1314–1340.

(67) Plötner, J. r.; Tozer, D. J.; Dreuw, A. *J. Chem. Theory Comput.* **2010**, *6*, 2315–2324.

(68) Yanai, T.; Tew, D. P.; Handy, N. C. *Chem. Phys. Lett.* **2004**, *393*, 51–57.

(69) Tapavicza, E.; Meyer, A. M.; Furche, F. *Phys. Chem. Chem. Phys.* **2011**, *13*, 20986–20998.

(70) Tapavicza, E.; Bellchambers, G. D.; Vincent, J. C.; Furche, F. *Phys. Chem. Chem. Phys.* **2013**, *15*, 18336–18348.

(71) Bonačić-Koutecký, V.; Mitrić, R. *Chem. Rev.* **2004**, *105*, 11–66.

(72) Barbatti, M.; Lan, Z.; Crespo-Otero, R.; Szymczak, J. J.; Lischka, H.; Thiel, W. *J. Chem. Phys.* **2012**, *137*, 22A503.

(73) Plasser, F.; Crespo-Otero, R.; Pederzoli, M.; Pittner, J.; Lischka, H.; Barbatti, M. *J. Chem. Theory Comput.* **2014**, *10*, 1395–1405.

(74) Gao, X.; Peng, Q.; Niu, Y.; Wang, D.; Shuai, Z. *Phys. Chem. Chem. Phys.* **2012**, *14*, 14207–14216.

(75) Crespo-Hernández, C. E.; Cohen, B.; Hare, P. M.; Kohler, B. *Chem. Rev.* **2004**, *104*, 1977–2020.

(76) Gascon, J. A.; Batista, V. S. *Biophys. J.* **2004**, *87*, 2931–2941.

(77) Eckert-Maksic, M.; Vazdar, M.; Ruckenbauer, M.; Barbatti, M.; Muller, T.; Lischka, H. *Phys. Chem. Chem. Phys.* **2010**, *12*, 12719–12726.

(78) Ruckenbauer, M.; Barbatti, M.; Sellner, B.; Muller, T.; Lischka, H. *J. Phys. Chem. A* **2010**, *114*, 12585–12590.

(79) Ruckenbauer, M.; Barbatti, M.; Muller, T.; Lischka, H. *J. Phys. Chem. A* **2013**, *117*, 2790–2799.

(80) Warshel, A.; Levitt, M. *J. Mol. Biol.* **1976**, *103*, 227–249.

(81) Plasser, F.; Lischka, H. *Photochem. Photobiol. Sci.* **2013**, *12*, 1440–52.

(82) Plasser, F.; Aquino, A. J.; Hase, W. L.; Lischka, H. *J. Phys. Chem. A* **2012**, *116*, 11151–60.

(83) Antol, I.; Eckert-Maksic, M.; Vazdar, M.; Ruckenbauer, M.; Lischka, H. *Phys. Chem. Chem. Phys.* **2012**, *14*, 13262–13272.

(84) Punwong, C.; Owens, J.; Martinez, T. J. *J. Phys. Chem. B* **2014**, 704–714.

(85) Lan, Z.; Lu, Y.; Fabiano, E.; Thiel, W. *ChemPhysChem* **2011**, *12*, 1989–1998.

(86) Widmalm, G.; Pastor, R. W. *Faraday Trans.* **1992**, *88*, 1747−1754.
(87) Pastor, R. W.; Brooks, B. R.; Szabo, A. *Mol. Phys.* **1988**, *65*, 1409−1419.
(88) Cattaneo, P.; Granucci, G.; Persico, M. *J. Phys. Chem. A* **1999**, *103*, 3364−3371.
(89) Malhado, J. o. P.; Spezia, R.; Hynes, J. T. *J. Phys. Chem. A* **2010**, *115*, 3720−3735.
(90) Nelson, T.; Fernandez-Alberti, S.; Chernyak, V.; Roitberg, A. E.; Tretiak, S. *J. Chem. Phys.* **2012**, *136*, 054108.
(91) Schwerdtfeger, C. A.; Soudackov, A. V.; Hammes-Schiffer, S. *J. Chem. Phys.* **2014**, *140*, 034113.
(92) Persico, M.; Granucci, G. *Theor. Chem. Acc.* **2014**, *133*, 1−28.
(93) Doltsinis, N. L.; Marx, D. *Phys. Rev. Lett.* **2002**, *88*, 166402.
(94) Furche, F.; Ahlrichs, R.; Hättig, C.; Klopper, W.; Sierka, M.; Weigend, F. *Wiley Interdiscip. Rev.: Comput. Mol. Sci.* **2014**, *4*, 91−100.
(95) Fabiano, E.; Keal, T. W.; Thiel, W. *Chem. Phys.* **2008**, *349*, 334−347.
(96) Werner, H.-J.; Knowles, P. J.; Knizia, G.; Manby, F. R.; Schütz, M. *Wiley Interdiscip. Rev.: Comput. Mol. Sci.* **2012**, *2*, 242−253.
(97) Akimov, A. V.; Prezhdo, O. V. *J. Chem. Theory Comput.* **2013**, *9*, 4959−4972.
(98) Richter, M.; Marquetand, P.; González-Vázquez, J. s.; Sola, I.; González, L. *J. Chem. Theory Comput.* **2011**, *7*, 1253−1258.
(99) Barbatti, M.; Granucci, G.; Persico, M.; Ruckenbauer, M.; Vazdar, M.; Eckert-Maksić, M.; Lischka, H. *J. Photoch. Photobio. A* **2007**, *190*, 228−240.
(100) Barbatti, M.; Granucci, G.; Persico, M.; Pittner, J.; Ruckenbauer, M.; Lischka, H. NEWTON-X: A package for Newtonian dynamics close to the crossing seam. Available at www.newtonx.org (accessed 2014.11.10).
(101) Martínez-Fernández, L.; González-Vázquez, J.; González, L.; Corral, I. *J. Chem. Theory Comput.* **2014**, 406−414.
(102) Ahlrichs, R.; Bär, M.; Häser, M.; Horn, H.; Kölmel, C. *Chem. Phys. Lett.* **1989**, *162*, 165−169.
(103) Frisch, M. J.; Trucks, G. W.; Schlegel, H. B.; Scuseria, G. E.; Robb, M. A.; Cheeseman, J. R.; Scalmani, G.; Barone, V.; Mennucci, B.; Petersson, G. A.; Nakatsuji, H.; Caricato, M.; Li, X.; Hratchian, H. P.; Izmaylov, A. F.; Bloino, J.; Zheng, G.; Sonnenberg, J. L.; Hada, M.; Ehara, M.; Toyota, K.; Fukuda, R.; Hasegawa, J.; Ishida, M.; Nakajima, T.; Honda, Y.; Kitao, O.; Nakai, H.; Vreven, T.; Montgomery Jr., J. A.; Peralta, J. E.; Ogliaro, F.; Bearpark, M. J.; Heyd, J.; Brothers, E. N.; Kudin, K. N.; Staroverov, V. N.; Kobayashi, R.; Normand, J.; Raghavachari, K.; Rendell, A. P.; Burant, J. C.; Iyengar, S. S.; Tomasi, J.; Cossi, M.; Rega, N.; Millam, N. J.; Klene, M.; Knox, J. E.; Cross, J. B.; Bakken, V.; Adamo, C.; Jaramillo, J.; Gomperts, R.; Stratmann, R. E.; Yazyev, O.; Austin, A. J.; Cammi, R.; Pomelli, C.; Ochterski, J. W.; Martin, R. L.; Morokuma, K.; Zakrzewski, V. G.; Voth, G. A.; Salvador, P.; Dannenberg, J. J.; Dapprich, S.; Daniels, A. D.; Farkas, Ö.; Foresman, J. B.; Ortiz, J. V.; Cioslowski, J.; Fox, D. J. *Gaussian 09*; Gaussian, Inc.: Wallingford, CT, 2009.
(104) Schmidt, M. W.; Baldridge, K. K.; Boatz, J. A.; Elbert, S. T.; Gordon, M. S.; Jensen, J. H.; Koseki, S.; Matsunaga, N.; Nguyen, K. A.; Su, S.; Windus, T. L.; Dupuis, M.; Montgomery, J. A. *J. Comput. Chem.* **1993**, *14*, 1347−1363.
(105) Swope, W. C.; Andersen, H. C.; Berens, P. H.; Wilson, K. R. *J. Chem. Phys.* **1982**, *76*, 637−649.
(106) Verlet, L. *Phys. Rev.* **1967**, *159*, 98−103.
(107) Hammes-Schiffer, S.; Tully, J. C. *J. Chem. Phys.* **1994**, *101*, 4657−4667.
(108) Schwartz, B. J.; Bittner, E. R.; Prezhdo, O. V.; Rossky, P. J. *J. Chem. Phys.* **1996**, *104*, 5942−5955.
(109) Hack, M. D.; Truhlar, D. G. *J. Chem. Phys.* **2001**, *114*, 9305−9314.
(110) Cheng, S. C.; Zhu, C.; Liang, K. K.; Lin, S. H.; Truhlar, D. G. *J. Chem. Phys.* **2008**, *129*, 024112.
(111) Li, B.; Chu, T.-S.; Han, K.-L. *J. Comput. Chem.* **2010**, *31*, 362−370.
(112) Granucci, G.; Persico, M. *J. Chem. Phys.* **2007**, *126*, 134114.
(113) Zhu, C.; Jasper, A. W.; Truhlar, D. G. *J. Chem. Theory Comput.* **2005**, *1*, 527−540.
(114) Thachuk, M.; Ivanov, M. Y.; Wardlaw, D. M. *J. Chem. Phys.* **1998**, *109*, 5747−5760.
(115) Granucci, G.; Persico, M.; Zoccante, A. *J. Chem. Phys.* **2010**, *133*, 134111.
(116) Subotnik, J. E.; Shenvi, N. *J. Chem. Phys.* **2011**, *134*, 024105.
(117) Ouyang, W.; Subotnik, J. E. *J. Chem. Phys.* **2014**, *140*, 204102.
(118) Herman, M. F. *J. Chem. Phys.* **1984**, *81*, 754−763.
(119) Tavernelli, I.; Tapavicza, E.; Rothlisberger, U. *J. Mol. Struct. THEOCHEM* **2009**, *914*, 22−29.
(120) Chernyak, V.; Mukamel, S. *J. Chem. Phys.* **2000**, *112*, 3572−3579.
(121) Baer, R. *Chem. Phys. Lett.* **2002**, *364*, 75−79.
(122) Hu, C.; Hirai, H.; Sugino, O. *J. Chem. Phys.* **2007**, *127*, 064103.
(123) Hu, C.; Hirai, H.; Sugino, O. *J. Chem. Phys.* **2008**, *128*, 154111.
(124) Hu, C.; Sugino, O.; Tateyama, Y. *J. Chem. Phys.* **2009**, *131*, 114101.
(125) Tapavicza, E.; Tavernelli, I.; Rothlisberger, U. *Phys. Rev. Lett.* **2007**, *98*, 023001.
(126) Tavernelli, I.; Curchod, B. F.; Laktionov, A.; Rothlisberger, U. *J. Chem. Phys.* **2010**, *133*, 194104.
(127) Send, R.; Furche, F. *J. Chem. Phys.* **2010**, *132*, 044107.
(128) Li, Z.; Liu, W. *J. Chem. Phys.* **2014**, *141*, 014110.
(129) Ou, Q.; Alguire, E. C.; Subotnik, J. E. *J. Phys. Chem. B* **2014**, DOI: 10.1021/jp505767b.
(130) Alguire, E. C.; Ou, Q.; Subotnik, J. E. *J. Phys. Chem. B* **2014**, DOI: 10.1021/jp5057682.
(131) Ou, Q.; Fatehi, S.; Alguire, E.; Shao, Y.; Subotnik, J. E. *J. Chem. Phys.* **2014**, *141*, 024114.
(132) Zhang, X.; Herbert, J. M. *J. Chem. Phys.* **2014**, *141*, 064104.
(133) Lischka, H.; Dallos, M.; Shepard, R. *Mol. Phys.* **2002**, *100*, 1647−1658.
(134) Lischka, H.; Dallos, M.; Szalay, P. G.; Yarkony, D. R.; Shepard, R. *J. Chem. Phys.* **2004**, *120*, 7322−7329.
(135) Tavernelli, I.; Tapavicza, E.; Rothlisberger, U. *J. Chem. Phys.* **2009**, *130*, 124107.
(136) Mitric, R.; Werner, U.; Bonacic-Koutecky, V. *J. Chem. Phys.* **2008**, *129*, 164118.
(137) Casida, M. E. Time-Dependent Density Functional Response Theory for Molecules. In *Recent Advances in Density Functional Methods*; World Scientific Publishing: 1995; pp 155−192.
(138) Werner, U.; Mitrić, R.; Suzuki, T.; Bonačić-Koutecký, V. *Chem. Phys.* **2008**, *349*, 319−324.
(139) Tapavicza, E.; Tavernelli, I.; Rothlisberger, U.; Filippi, C.; Casida, M. E. *J. Chem. Phys.* **2008**, *129*, 124108.
(140) Noon, W. H.; Kong, Y.; Ma, J. *Proc. Natl. Acad. Sci. U. S. A.* **2002**, *99*, 6466−6470.
(141) Olson, M. A.; Chaudhury, S.; Lee, M. S. *J. Comput. Chem.* **2011**, 32, 3014−3022.
(142) Wigner, E. *Phys. Rev.* **1932**, *40*, 749−759.
(143) Crespo-Otero, R.; Barbatti, M. *Theor. Chem. Acc.* **2012**, *131*, 1−14.
(144) Barbatti, M.; Aquino, A. J. A.; Lischka, H. *Phys. Chem. Chem. Phys.* **2010**, *12*, 4959−4967.
(145) Mitrić, R.; Hartmann, M.; Stanca, B.; Bonačić-Koutecký, V.; Fantucci, P. *J. Phys. Chem. A* **2001**, *105*, 8892−8905.
(146) Tannor, D. *Introduction to Quantum Mechanics: A Time-dependent Perspective*; Young, L., Ed.; University Science Books: 2007; pp 55−67.
(147) O'Connell, R. F. Wigner Distribution. In *Compendium of Quantum Physics*, Greenberger, D.; Hentschel, K.; Weinert, F., Eds.; Springer: Berlin, 2009; pp 851−854.
(148) Sels, D.; Brosens, F. *Phys. Rev. E* **2013**, *88*, 042101.
(149) Müller, U.; Stock, G. *J. Chem. Phys.* **1997**, *107*, 6230−6245.
(150) Peslherbe, G. H.; Wang, H.; Hase, W. L. Monte Carlo Sampling for Classical Trajectory Simulations. In *Advances in Chemical Physics*; John Wiley & Sons, Inc.: 2007; pp 171−201.

(151) Doubleday, C.; Bolton, K.; Hase, W. L. *J. Phys. Chem. A* **1998**, *102*, 3648−3658.
(152) Xu, L.; Doubleday, C. E.; Houk, K. N. *J. Am. Chem. Soc.* **2011**, *133*, 17848−17854.
(153) Granucci, G.; Persico, M. *J. Chem. Phys.* **2007**, *126*, 134114.
(154) Loncharich, R. J.; Brooks, B. R.; Pastor, R. W. *Biopolymers* **1992**, *32*, 523−535.
(155) Du, L.; Gao, J.; Liu, Y.; Liu, C. *J. Phys. Chem. B* **2012**, *116*, 11837−11844.
(156) Li, Y.; Shi, X.; Zhang, Q.; Hu, J.; Chen, J.; Wang, W. *Environ. Sci. Technol.* **2014**, *48*, 5008−5016.
(157) Barbatti, M.; Aquino, A. J. A.; Lischka, H. *Mol. Phys.* **2006**, *104*, 1053−1060.
(158) Gai, F.; Hasson, K. C.; McDonald, J. C.; Anfinrud, P. A. *Science* **1998**, *279*, 1886−1891.
(159) Yamazaki, S.; Kato, S. *J. Chem. Phys.* **2005**, *123*, 114510.
(160) Barbatti, M.; Pittner, J.; Pederzoli, M.; Werner, U.; Mitrić, R.; Bonačić-Koutecký, V.; Lischka, H. *Chem. Phys.* **2010**, *375*, 26−34.
(161) Bhattacharya, S.; Mula, S.; Chattopadhyay, S.; Banerjee, M. *J. Solution Chem.* **2006**, *35*, 1255−1269.
(162) Lorentzen, J. D.; Guha, S.; Menéndez, J.; Giannozzi, P.; Baroni, S. *Chem. Phys. Lett.* **1997**, *270*, 129−134.
(163) Torralva, B.; Niehaus, T. A.; Elstner, M.; Suhai, S.; Frauenheim, T.; Allen, R. E. *Phys. Rev. B* **2001**, *64*, 153105.
(164) Lippert, E.; Lüder, W.; Moll, F.; Nägele, W.; Boos, H.; Prigge, H.; Seibold-Blankenstein, I. *Angew. Chem.* **1961**, *73*, 695−706.
(165) Rettig, W. *Angew. Chem., Int. Ed.* **1986**, *25*, 971−988.
(166) Bhattacharyya, K.; Chowdhury, M. *Chem. Rev.* **1993**, *93*, 507−535.
(167) Lippert, E.; Rettig, W.; Bonačić-Koutecký, V.; Heisel, F.; Miehé, J. A. *Adv. Chem. Phys.* **1987**, *68*, 1.
(168) Rotkiewicz, K.; Grellmann, K. H.; Grabowski, Z. R. *Chem. Phys. Lett.* **1973**, *19*, 315−318.
(169) Sobolewski, A. L.; Sudholt, W.; Domcke, W. *J. Phys. Chem. A* **1998**, *102*, 2716−2722.
(170) Park, M.; Kim, C. H.; Joo, T. *J. Phys. Chem. A* **2012**, *117*, 370−377.
(171) Druzhinin, S. I.; Ernsting, N. P.; Kovalenko, S. A.; Lustres, L. P.; Senyushkina, T. A.; Zachariasse, K. A. *J. Phys. Chem. A* **2005**, *110*, 2955−2969.
(172) Rettig, W.; Zietz, B. *Chem. Phys. Lett.* **2000**, *317*, 187−196.
(173) Rettig, W.; Fritz, R.; Braun, D. *J. Phys. Chem. A* **1997**, *101*, 6830−6835.
(174) Rettig, W.; Bliss, B.; Dirnberger, K. *Chem. Phys. Lett.* **1999**, *305*, 8−14.
(175) Demeter, A.; Druzhinin, S.; George, M.; Haselbach, E.; Roulin, J.-L.; Zachariasse, K. A. *Chem. Phys. Lett.* **2000**, *323*, 351−360.
(176) Fuß, W.; Pushpa, K. K.; Rettig, W.; Schmid, W. E.; Trushin, S. A. *Photochem. Photobiol. Sci.* **2002**, *1*, 255−262.
(177) Gómez, I.; Reguero, M.; Boggio-Pasqua, M.; Robb, M. A. *J. Am. Chem. Soc.* **2005**, *127*, 7119−7129.
(178) Fuß, W.; Schmid, W. E.; Kuttan Pushpa, K.; Trushin, S. A.; Yatsuhashi, T. *Phys. Chem. Chem. Phys.* **2007**, *9*, 1151−1169.
(179) Ernsting, N. P. *J. Phys. Chem.* **1985**, *89*, 4932−4939.
(180) Fang, C.; Frontiera, R. R.; Tran, R.; Mathies, R. A. *Nature* **2009**, *462*, 200−204.
(181) Sobolewski, A. L.; Domcke, W.; Hättig, C. *J. Phys. Chem. A* **2006**, *110*, 6301−6306.
(182) Stock, K.; Bizjak, T.; Lochbrunner, S. *Chem. Phys. Lett.* **2002**, *354*, 409−416.
(183) Lochbrunner, S.; Wurzer, A. J.; Riedle, E. *J. Phys. Chem. A* **2003**, *107*, 10580−10590.
(184) Takeuchi, S.; Tahara, T. *J. Phys. Chem. A* **2005**, *109*, 10199−10207.
(185) Schriever, C.; Barbatti, M.; Stock, K.; Aquino, A. J. A.; Tunega, D.; Lochbrunner, S.; Riedle, E.; de Vivie-Riedle, R.; Lischka, H. *Chem. Phys.* **2008**, *347*, 446−461.
(186) Stock, K.; Schriever, C.; Lochbrunner, S.; Riedle, E. *Chem. Phys.* **2008**, *349*, 197−203.
(187) Barbara, P. F.; Brus, L. E.; Rentzepis, P. M. *J. Am. Chem. Soc.* **1980**, *102*, 5631−5635.
(188) Bancewicz, T.; Głaz, W.; Kjelich, S. *Chem. Phys.* **1988**, *128*, 321−334.
(189) Barbatti, M.; Aquino, A. J. A.; Lischka, H.; Schriever, C.; Lochbrunner, S.; Riedle, E. *Phys. Chem. Chem. Phys.* **2009**, *11*, 1406−1415.
(190) Chou, P.-T.; Chen, Y.-C.; Yu, W.-S.; Chou, Y.-H.; Wei, C.-Y.; Cheng, Y.-M. *J. Phys. Chem. A* **2001**, *105*, 1731−1740.
(191) Martinez, M. L.; Cooper, W. C.; Chou, P.-T. *Chem. Phys. Lett.* **1992**, *193*, 151−154.
(192) Lee, J.; Kim, C. H.; Joo, T. *J. Phys. Chem. A* **2013**, *117*, 1400−1405.
(193) Higashi, M.; Saito, S. *J. Phys. Chem. Lett.* **2011**, *2*, 2366−2371.
(194) Kim, C. H.; Joo, T. *Phys. Chem. Chem. Phys.* **2009**, *11*, 10266−10269.
(195) Schriever, C.; Lochbrunner, S.; Ofial, A. R.; Riedle, E. *Chem. Phys. Lett.* **2011**, *503*, 61−65.
(196) Xu, X.; Yang, K. R.; Truhlar, D. G. *J. Chem. Theory Comput.* **2014**, *10*, 2070−2084.
(197) Bernard, Y. A.; Shao, Y.; Krylov, A. I. *J. Chem. Phys.* **2012**, *136*, 204103.
(198) Huix-Rotllant, M.; Natarajan, B.; Ipatov, A.; Muhavini Wawire, C.; Deutsch, T.; Casida, M. E. *Phys. Chem. Chem. Phys.* **2010**, *12*, 12811−12825.